Research Article

Meryem Hajji Nabih*, Hamza Boulika, Maryam El Hajam, Noureddine Idrissi Kandri, Maryam M. Alomran, Fehmi Boufahja

Development and characterization of new ecological adsorbents based on cardoon wastes: Application to brilliant green adsorption

https://doi.org/10.1515/chem-2024-0078
received May 31, 2024; accepted July 18, 2024

Abstract: This study aimed to develop four adsorbents, neat and activated, from the cardoon leaves and stems. The developed adsorbents were first analyzed to determine the surface acid–base properties using Boehm's method, pH at zero charge point, iodine and methylene blue values, and moisture, ash, and fixed carbon contents. They were also characterized by scanning electron microscopy coupled with energy-dispersive X-ray analysis, X-ray diffraction, Fourier transform infrared absorption spectroscopy, thermogravimetric analysis, and inductively coupled plasma atomic emission spectroscopy. After that, these adsorbents were applied for adsorption of an organic dye "brilliant green" (BG), and the effect of various parameters on the adsorption efficiency was evaluated. The obtained results revealed the differences between the adsorbents derived from the neat cardoon leaves and stems and their activated carbon in terms of properties and BG adsorption efficiency.

*** Corresponding author: Meryem Hajji Nabih,** Signals Systems and Components Laboratory (SSC), Faculty of Sciences and Techniques, Sidi Mohamed Ben Abdellah University, Route Imouzzer, BP2202, Atlas, FEZ, Morocco, e-mail: meryem.hajjinabih@usmba.ac.ma
Hamza Boulika: Signals Systems and Components Laboratory (SSC), Faculty of Sciences and Techniques, Sidi Mohamed Ben Abdellah University, Route Imouzzer, BP2202, Atlas, FEZ, Morocco, e-mail: hamza.boulika@usmba.ac.ma
Maryam El Hajam: Advanced Structures and Composites Center, University of Maine, Orono, 04469, United States of America, e-mail: maryam.el1@maine.edu
Noureddine Idrissi Kandri: Signals, Systems and Components Laboratory (SSC), Faculty of Sciences and Techniques, Sidi Mohamed Ben Abdellah University, Route Imouzzer, BP2202, Atlas, FEZ, Morocco, e-mail: noureddine.idrissikandri@usmba.ac.ma
Maryam M. Alomran: Department of Biology, College of Science, Princess Nourah bint Abdulrahman University, P.O. Box 84428, Riyadh, 11671, Saudi Arabia, e-mail: mmalomran@pnu.edu.sa
Fehmi Boufahja: Biology Department, College of Science, Imam Mohammad Ibn Saud Islamic University (IMSIU), Riyadh, 11623, Saudi Arabia, e-mail: faboufahja@imamu.edu.sa

Keywords: depollution, kinetics, isotherms, ecology, environment

1 Introduction

Cardoon is a plant species of the Asteraceae family (*Cynara cardunculus* L.), which has recently attracted the interest of food and pharmaceutical industries, whether cultivated or wild [1,2]. Its derivatives can be used as a vegetable coagulant in the production of certain cheeses, paper pulp, and edible oil [1–3]. The many industrial applications of this plant produce millions of tons of waste [4] which pollute the environment. However, these wastes are an important source of biologically active compounds such as antioxidants [4], making them potential precursors for the preparation of environmentally friendly adsorbents for the reduction and even elimination of organic dyes contained in industrial effluents, mainly those from textiles [5–7]. Several physico-chemical processes have been used to treat organic dyes, such as adsorption [8–10], coagulation-flocculation, membrane filtration [11], and adsorption on commercially activated carbon. However, only adsorption remains industrially exploitable and eco-compatible. As a result, scientists are constantly looking for adsorbents that are cheaper, easier to prepare, and more effective than commercial activated carbons. A variety of plant wastes have recently been used to develop environmentally friendly adsorbents and tested for optimal adsorption in water and industrial effluent treatment [12,13]. The aim of this study was to develop four adsorbents from the leaves and stems of crude and activated cardoon wastes. The prepared materials' moisture, ash, and fixed carbon contents were determined, along with surface acid–base functions, pH at zero charge point (pH_{PZC}), and iodine and methylene blue values. Characterization by energy-dispersive X-ray spectroscopy coupled with scanning electron microscopy (EDX-SEM), X-ray diffraction (XRD), Fourier transform infrared (FTIR) absorption spectroscopy, inductively coupled plasma atomic emission spectroscopy

(ICP-AES), and thermogravimetric analysis (TGA) was also carried out. Their adsorption efficiency was evaluated and optimized using a solution of brilliant green (BG). The effects of solution pH, adsorbent mass, contact time, initial dye concentration, medium temperature, and salinity were studied, along with their kinetics and BG adsorption.

2 Materials and methods

2.1 Materials

After being gathered from a vegetable market in Fez, Morocco, vegetable waste from *C. cardunculus* L. was cleaned, dried, separated into leaves and stems, ground, and sieved to a diameter of between 50 µm and 0.2 mm. They were then Soxhlet extracted in a solvent [4]. The leaf and stem residues resulting from this extraction were divided into two parts: the first was washed with distilled water, filtered, and oven-dried at 110°C to obtain ecological adsorbents denoted as AdsF for the leaves and AdsT for the stems. The second part was chemically and physically activated to obtain activated carbon, denoted as CAF for leaves and CAT for stems. Chemical activation was carried out on a mass of residue using a 30% volume of H_3PO_4. At room temperature, the resultant mixture was swirled for 24 h. After Büchner filtration, the residue was neutralized with water and oven-dried for 24 h. Physical activation was carried out as follows: the obtained dry product was placed in a Lenton furnace – a type of muffle furnace. The thermal cycle took place in two stages lasting one and a half hours at 180°C and one and a half hours at 350°C with an increase of 5°C/min in the heating rate [6–14]. Yields of ecological adsorbents and activated carbons were calculated from equation (1):

$$\text{Yield (\%)} = \frac{\text{Final mass}}{\text{Initial mass}} \times 100. \quad (1)$$

2.2 Characterization methods

2.2.1 Preliminary analysis

Using the ASTMD standard technique 2867-99, we determined the moisture and volatile matter content of various samples. The ash content was determined using the ASTMD standard technique 2867-94. The fixed carbon content was obtained by deducting the moisture, volatile matter, and ash contents from 100% [15].

2.2.2 Quantification of surface oxygen groups using Boehm's method and pH_{PZC}

Boehm's method was used to determine the acidic or basic nature of the adsorbents' surface. The graphical method for detecting pH_{PZC} uses curves of the final pH values (pH_f) as a function of initial pH values (pH_i) [6].

2.2.3 Iodine value and methylene blue value

The quantity of iodine adsorbed by the developed materials was evaluated using the standard method (AWWA B600-76) [16]. Quantification of the methylene blue index for the four adsorbents was carried out using the CEFIC 1989 method [17].

2.2.4 Characterization by physicochemical methods

Adsorbents' surface morphology and porosity were analyzed using a JEOL-IT500 HR scanning electron microscope, coupled with an EDX spectrometer for the qualitative determination of their constituent compounds. An X-ray diffractometer Panalytical X'Pert Pro was used to identify the crystal structure. The bonds of the functional groups present in the chemical composition of the adsorbents were identified using a Bruker Vertex 70 FTIR spectrophotometer in ATR mode. Elemental analysis was carried out by ICP-AES using a Horiba Jobin-Yvon Activa type [18]. A LINSEIS high-end thermobalance (TG + DSC) (LINSEIS STA PT 1600) was used to test the adsorbents' thermal stability between 20 and 1,000°C at a heating rate of 10°C/min.

2.3 Adsorption process

The Batch technique was used for adsorption experiments [6]. A dye solution with a concentration of C_0 having a volume V and an adsorbent mass m distributed throughout it was used. After 30 min of stirring, the mixture was centrifuged. Using a UV spectrophotometer, the equilibrium concentration of C_e dye in the filtrate was ascertained spectrophotometrically.

The quantity of dye adsorbed q_e was determined by equation (2):

$$q_e = \frac{C_0 - C_e}{m} \times V. \quad (2)$$

Adsorption percentage of dye (% Ads) was calculated by formula (3):

$$\% \text{ Ads} = \frac{C_0 - C_e}{C_0} \times 100. \quad (3)$$

2.3.1 Kinetics and isotherm of adsorption

2.3.1.1 Adsorption kinetics

The BG dye's adsorption kinetics was investigated on the AdsF (ecological adsorbent made from raw leaves), AdsT (ecological adsorbent made from raw stems), CAF (ecological adsorbent based on chemically and physically activated leaves), and CAT (ecological adsorbent based on chemically and physically activated stems) samples. The correlation between the experimental results and those of the kinetic model forms the basis of this study. Namely:

- The Lagergren model (pseudo-first order – PFO) determined by equation (4) [19]:

$$\ln(q_e - q_t) = \ln(q_e) - K_1 \cdot t, \quad (4)$$

where K_1 is the pseudo-first-order kinetic constant in min^{-1}, q_t is the quantity of BG adsorbed at time t in mg/g, q_e is the quantity of BG adsorbed in equilibrium in mg/g, and t is the contact time in min.

- The Blanchard model (pseudo-second order – PSO) determined by equation (5) [20]:

$$\frac{t}{q_t} = \frac{1}{K_2 \cdot q_e^2} + \frac{1}{q_e} \cdot t, \quad (5)$$

where K_2 is the rate constant for the second-order adsorption reaction of the dye on the adsorbent in g mg^{-1} min^{-1}.

The R^2 correlation coefficients and the values of the theoretical and experimental maximal quantities were used to assess the consistency between experimental results and those predicted by these models.

2.3.1.2 Adsorption isotherms

We selected the two most popular models, the Freundlich and Langmuir models, to simulate adsorption isotherms.

- The Langmuir model is defined by formula (6) [21]:

$$\frac{C_e}{q_e} = \frac{1}{q_{max}} \cdot C_e + \frac{1}{q_{max} \cdot K_L}, \quad (6)$$

where q_e is the quantity of dye adsorbed at equilibrium in mg/g, C_e is the concentration of dye at equilibrium in mg/L, and K_L is the thermodynamic equilibrium constant for adsorption in L/mg.

- The Freundlich model is represented by formula (7) [22]:

$$\text{Log}(q_e) = \text{Log}(K_f) + \frac{1}{n_f} \cdot \text{Log}(C_e), \quad (7)$$

where K_f is the Freundlich constant and n_f is the adsorption intensity.

3 Results and discussion

3.1 Adsorbent characterization

3.1.1 Preliminary analysis

The preliminary analysis results in Table 1 show that AdsF and AdsT raw adsorbents have lower moisture, ash, and fixed carbon contents than CAF and CAT. However, the volatile matter content is lower for CAF and CAT. Alongamo et al. found that the peelings of "cassava tubers" produced distinct outcomes when it came to activated carbon.

3.1.2 Quantification of surface oxygen groups using Boehm's method and pH_{PZC}

3.1.2.1 Acid–base character: Boehm's method

The results obtained from the acid–base analysis of the surface functions of the adsorbent show that the acid functions predominate, with CAF and CAT being more acidic. Similar results were obtained for activated carbon prepared from "coffee waste" (Table 2).

3.1.2.2 pH_{PZC}

The results of pH_{PZC} in Figure 1 indicate that the pH_{PZC} values obtained for AdsF and AdsT are 6.8 and 5.8, respectively. However, the pH_{PZC} values for CAF and CAT are in the order of 4.9 and 6.2, respectively; this shows that all four adsorbents are acidic in character. When the pH falls below the pH_{PZC} value, the adsorbent surface is positively charged; when the pH rises over the pH_{PZC} value, it is negatively charged. The density of negatively charged ions on the adsorbent surface rises as the pH moves closer to pH_{PZC}. These results concur with those of surface functional group quantification. Benadjemia et al. found similar outcomes with activated carbon made from artichoke leaves [24].

Table 1: Results of preliminary analyses of AdsF, AdsT, CAF, and CAT

Adsorbents	Moisture (%)	Volatile matter (%)	Ash (%)	Fixed carbon (%)
AdsF	1.11	90.32	4.96	3.61
AdsT	2.50	88.28	5.09	4.13
CAF	1.50	23.67	10.69	64.14
CAT	2.91	20.53	21.34	55.22
Cassava tubers [15]	1	13	8	78

Table 2: Surface oxygen group quantification using the Boehm method

Adsorbents	AdsF	AdsT	CAF	CAT	Coffee waste [23]
Total acidity (meq·g^{-1})	2.890	2.425	4.500	3.500	2.573
Total basicity (meq·g^{-1})	1.635	1.585	2.075	2.400	2.015

3.1.3 Iodine and methylene blue indices

The iodine values obtained for AdsF, AdsT, CAF, and CAT are 437.40, 400.17, 500.34, and 504.91 mg/g, respectively. These values show that the developed adsorbents are microporous in nature according to ASTMD 2866-94 [16]. The methylene blue indices of AdsF, AdsT, CAF, and CAT are of the order of 4.27, 3.09, 4.62, and 4.68 in mg/g, respectively. These show that these materials also have a mesoporous and macroporous nature [17].

3.1.4 Physicochemical characterization

3.1.4.1 SEM observation

SEM observation in Figure 2a and b of non-activated adsorbents reveals a heterogeneous porous surface with pore diameters ranging from 0.8928 to 2.525 µm for AdsF and from 3.718 to 6.445 µm for AdsT. Chemical activation followed by calcination in Figure 2c and d results in activated adsorbents with homogeneous pore structures and a rough surface texture, with diameters of 2.720–8.595 µm for CAF and 2.035–5.398 µm for CAT. This activation improves the surface texture of the raw adsorbents and develops active cavities. Artichoke leaves activated carbon illustrations display rather uneven surfaces with diameters ranging from 10 to 200 µm [24].

Qualitative analysis by surface electron scattering (EDX) (Table 3) shows a dominance of carbon and oxygen in the adsorbents, justifying their organic character. The oxygen content falls and the carbon content rises in activated adsorbents compared with those in non-activated ones. These results show that CAF and CAT are essentially made up of carbon graphite. The activation of the H_3PO_4 solution, which interacted with the acid functions of the adsorbent surface, is responsible for the significant amount of phosphorus present on the surface of CAF and CAT [25]. The outcomes for the activated carbon made from *Gundelia tournefortii* seeds show a carbon content of 37.35% and an oxygen content of 41.55%. These results differ from those reported by Mokhtaryan et al. [26].

3.1.4.2 X-ray diffraction (XRD)

The diffractograms of AdsF and CAF display similar peaks. Figure 3 shows a large intense peak between 20 and 25° in

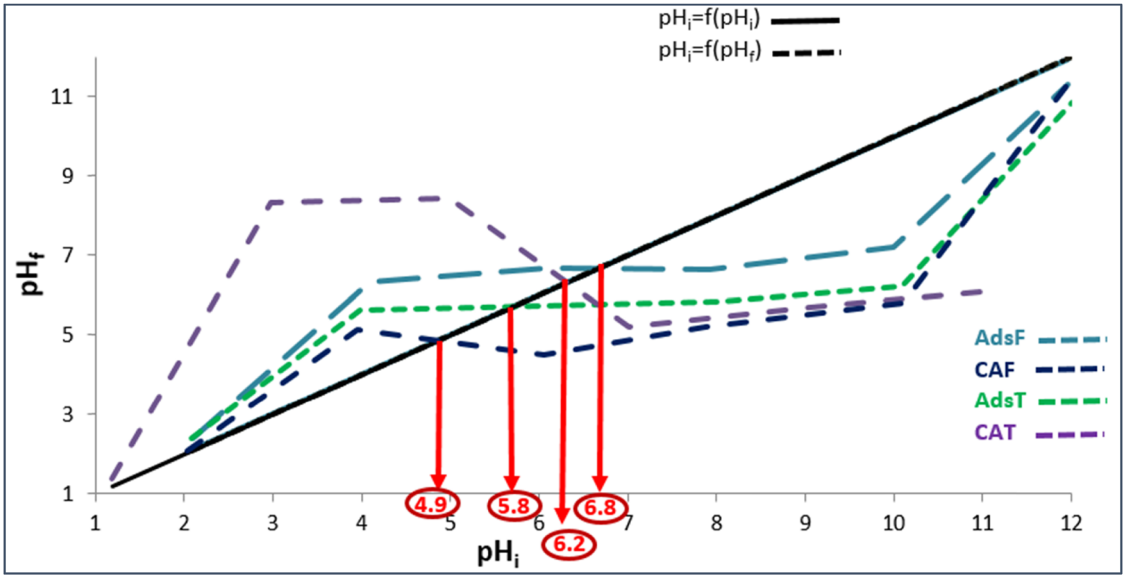

Figure 1: pH_{PZC} of AdsF, AdsT, CAF, and CAT.

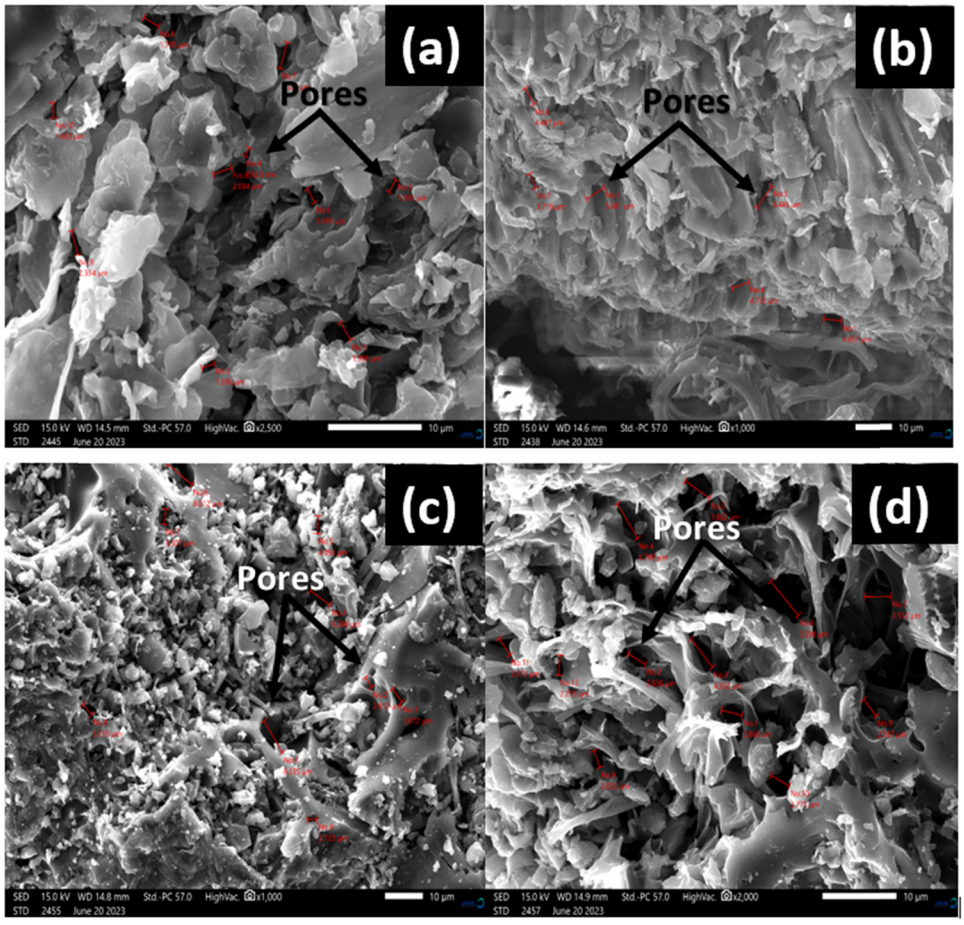

Figure 2: Surface morphology of AdsF (a), AdsT (b), CAF (c), and CAT (d).

2θ, which is attributed to the (002) crystalline plane of amorphous carbon [6]. There are two centered, less intense peaks at 31 and 49° in 2θ, corresponding, respectively, to the (040) and (102) planes of crystalline graphite. However for AdsF, there are peaks at 42, 44, and 45° in 2θ corresponding to the (101) plane of crystalline graphite [25]. The diffractograms of AdsT and CAT are almost similar in terms of peaks; they show two broad peaks between 10 and 15° and between 20 and 25° in 2θ; the latter are attributed to the (101) and (002) crystal planes, respectively, of amorphous carbon [6] and another peak at 34° in 2θ corresponding to the (040) plane of crystalline graphite. These outcomes resemble those of activated carbon made from almond shells [25].

3.1.4.3 Fourier transform infrared (FTIR) spectroscopy

IR spectroscopic analysis of AdsF, AdsT, CAF, and CAT in the 400–4,000 cm^{-1} range enables the detection of adsorbent organic functional groups. In this way, analysis of the

Table 3: EDX microanalysis of the elements present in AdsF, AdsT, CAF, and CAT

Elements	Mass (%)			
	AdsF	AdsT	CAF	CAT
C	59.10 ± 0.18	49.96 ± 0.16	80.03 ± 0.52	86.72 ± 0.18
O	37.14 ± 0.41	47.18 ± 0.39	15.86 ± 0.71	11.85 ± 0.24
Mg	0.28 ± 0.03	0.45 ± 0.04	00.00 ± 0.00	00.00 ± 0.00
Ca	3.28 ± 0.11	2.41 ± 0.08	00.00 ± 0.00	00.00 ± 0.00
P	0.21 ± 0.03	00.00 ± 0.00	2.78 ± 0.18	1.00 ± 0.04
Si	00.00 ± 0.00	00.00 ± 0.00	1.34 ± 0.13	0.44 ± 0.03

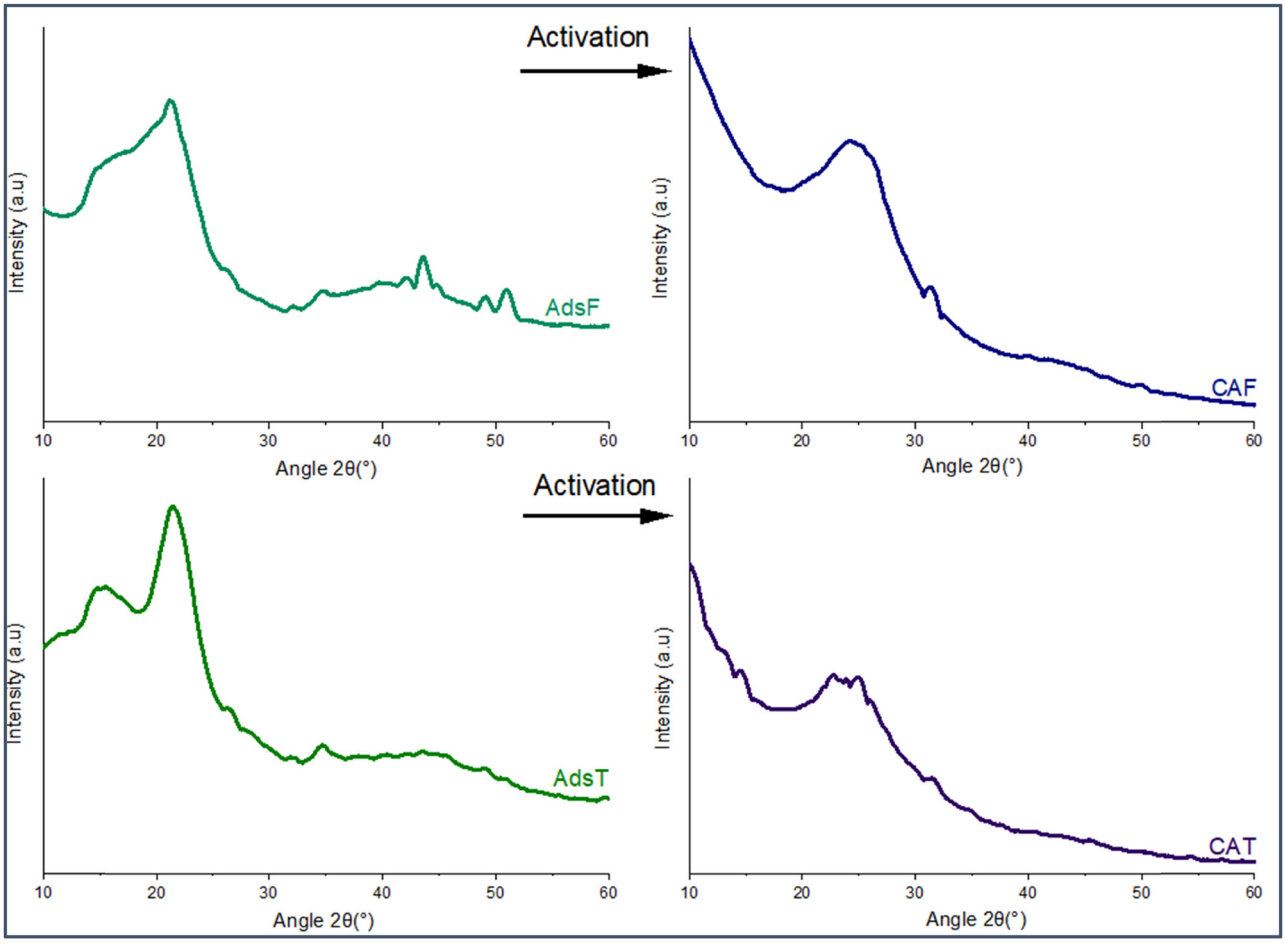

Figure 3: Diffractograms of AdsF, AdsT, CAF, and CAT.

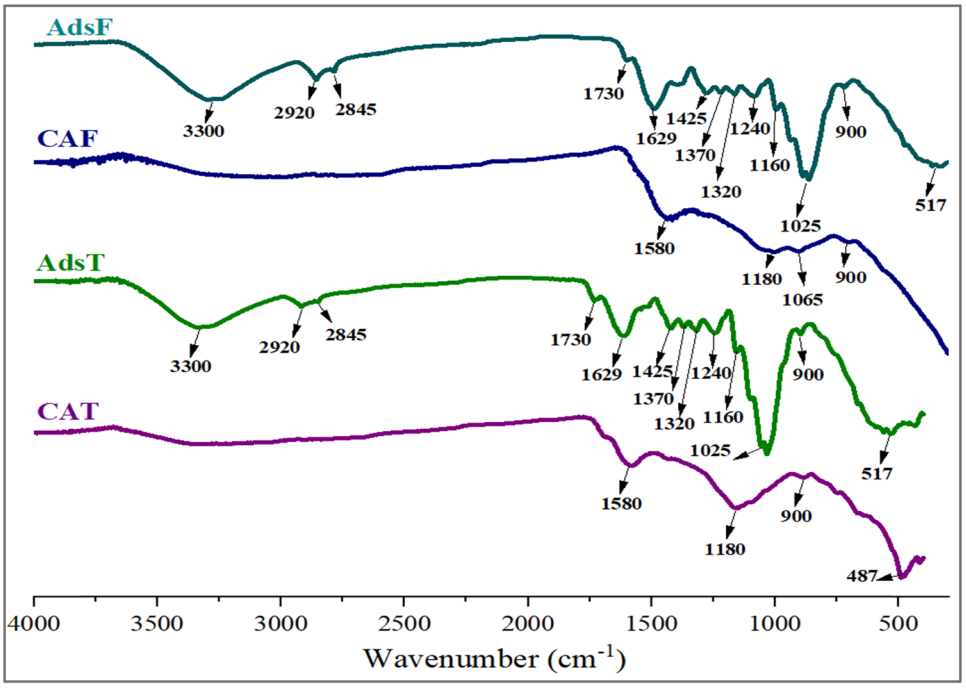

Figure 4: FTIR spectra of AdsF, CAF, AdsT, and CAT.

Table 4: Elemental compositions of AdsF, AdsT, CAF, and CAT

Elements (mg/g)	Ca	Mg	P	Fe	Al	Na
AdsF	15.537	2.304	1.025	0.362	0.356	0.201
CAF	20.904	7.927	5.464	0.553	0.783	1.497
AdsT	21.738	3.348	0.521	0.206	0.313	0.818
CAT	46.658	20.560	13.191	0.740	1.098	3.112
Elements (mg/g)	**Sr**	**Zn**	**K**	**Mn**	**Cu**	**Ba**
AdsF	0.180	0.119	0.155	0.032	0.030	0.024
CAF	0.043	0.026	0.309	0.000	0.040	0.027
AdsT	0.260	0.075	0.795	0.015	0.032	0.039
CAT	0.115	0.064	0.717	0.000	0.046	0.069

neat and activated adsorbent surfaces reveals the surface groups destroyed during activation. The IR absorption spectra of the prepared adsorbents in Figure 4 show a difference in the majority of absorption bands. The positions of the AdsF and AdsT absorption bands are similar but differ in intensity. They exhibit a broad absorption band with a center of 3,300 cm^{-1}, which is indicative of the hydroxyl functional groups of the water of hydration's O–H bond elongation. Absorption bands at 2,920 and 2,845 cm^{-1} indicate aliphatic C–H stretching of lignin and hemicellulose [27]. Another absorption band at 1,730 cm^{-1} is indicative of the xylan esters and/or carboxylic acids' C═O valence vibration, which are found in lignin and hemicelluloses [4]. The band centered at 1,629 cm^{-1} is attributed to the presence of strongly conjugated C–O in a quinone/carbonyl structure [27]. Another band at 1,425 cm^{-1} confirms the presence of the C–H bond. The existence of C–O and/or C–O–C bond stretching vibrations in acid groups is shown by the absorption band at 1,240 cm^{-1} [6]. Carboxylic acids show a broad band at 1,160 cm^{-1} corresponding to the in-plane deformation of aliphatic C–O bonds [25]. The band characteristic of cellulose at 1,025 cm^{-1} is more clear [4]. The absorption spectra of CAF and CAT reveal that chemical/physical activation leads to the disappearance of the main absorption bands of carboxylic acids and xylan esters present in hemicelluloses and lignin, due to solubilization during activation. For CAF and CAT, a band centered at 1,580 cm^{-1} is characteristic of P–O–C and P═OOH bonds [25]. A band at 1,180 cm^{-1} representing in-plane deformation of aliphatic C–O bonds is identified with the remaining carboxylic acids [25]. The stretching of the P–OH bond is responsible for the absorption band observed at 1,065 cm^{-1} in phosphonate groups [25]. Absorption bands at 900, 517, and 487 cm^{-1} correspond to the aromatic rings. In accord with preliminary analyses indicating the acidic nature of the surface, the results demonstrate the presence of acidic functional groups on the adsorbent surface.

3.1.4.4 ICP-AES

Elemental analysis results for AdsF, CAF, AdsT, and CAT reveal the presence of principal elements Ca, Mg, P, Fe, Al,

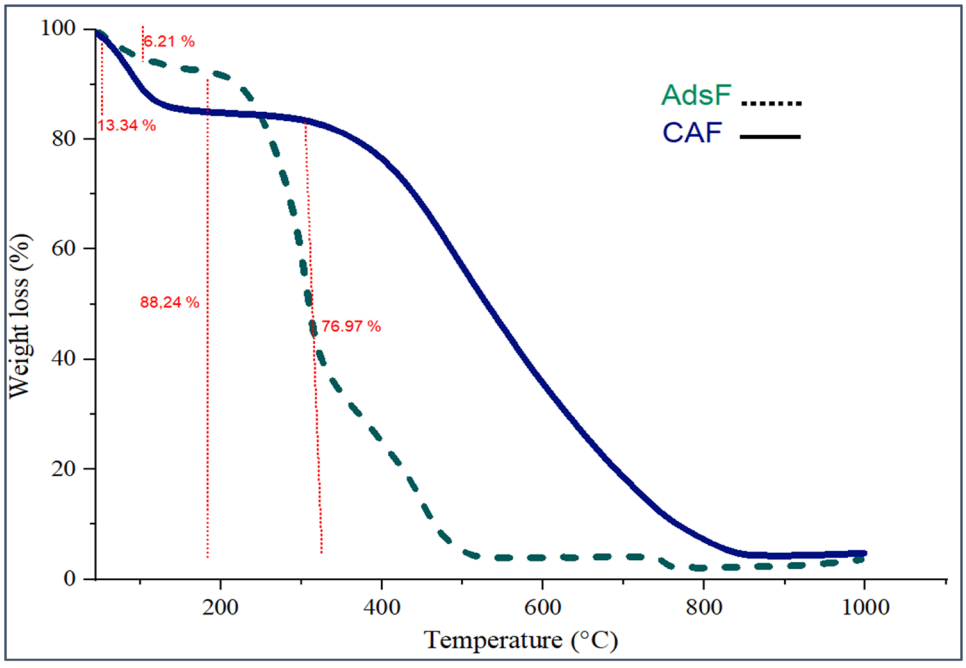

Figure 5: Thermograms (ATG) of AdsF and CAF.

and Na and traces of Sr, Zn, K, Mn, Cu, and Ba. Due to activation by H_3PO_4, residual phosphate is present in CAF and CAT, explaining their high phosphorus content (Table 4).

3.1.4.5 Thermogravimetric analysis

Thermograms of the neat and activated sheet adsorbents AdsF and CAF are shown in Figure 5 that demonstrate mass losses of 6.21 and 13.34%, respectively, at 90°C. These losses are caused by water vapor trapped in the pores of the processed adsorbents. AdsF and CAF show significant thermal stability between 125 and 180°C and 125 and 350°C, respectively, followed by a second, continuous, and significant mass loss of 88.24% in the range of 180–520°C for AdsF and 76.97% in the range of 350–850°C for CAF; the latter is due to the degradation of acid-function fragments bound to phosphates and polyphosphates.

Thermograms in Figure 6 of AdsT and CAT raw and activated rod-based adsorbents show that at 90°C there are mass losses of 8.15 and 7.15%, respectively; then, thermal stability is observed between 120 and 180°C for AdsT and between 120 and 350°C for CAT, followed by a second, significant, and continuous mass loss of 81.24% in the 180–510°C range for AdsT and 80% in the 350–680°C range for CAT. In conclusion, activated adsorbents are more thermally stable than non-activated ones. According to a study by Benadjemia et al., there is a first more marked mass loss at 400°C, a second less severe and progressive mass loss in the 400–600°C zone, and a third mass loss in the 650–850°C region [24].

3.1.4.6 Adsorbent production yield

The influence of H_3PO_4 treatment on the adsorbent yield was observed in the synthesis of adsorbents from neat and activated cardoon leaves and stems. Washing with distilled water gave yields of 56.56 and 51.42% for AdsF and AdsT, respectively, whereas with chemical activation followed by calcination, these yields increased to 60.00% for CAF and 83.71% for CAT. The influence of residual H_3PO_4 in the pores of CAF and CAT, which functions as a flame retardant throughout the carbonization process and provides a high yield, can be used to explain these yield disparities [28]. The volatile content released by activated adsorbents depends not only on the carbonization temperature but also on the activation conditions [24]. We also note that these yields vary between leaves and stems; indeed, we know from scanning electron microscopy that stems and leaves have different surface structures which influence their adsorbents' yields. Activated carbons with phosphoric acid made from artichoke waste gave comparable results [24].

3.2 Factors influencing BG adsorption

3.2.1 pH effect

Solutions of HCl and NaOH (0.1 M) were used to modify the pH values of the dye solutions between 3 and 10. Approximately 100 mg of adsorbent was dispersed in 25 ml of BG solution (80 ppm) for 30 min at 25°C, with gentle agitation. UV

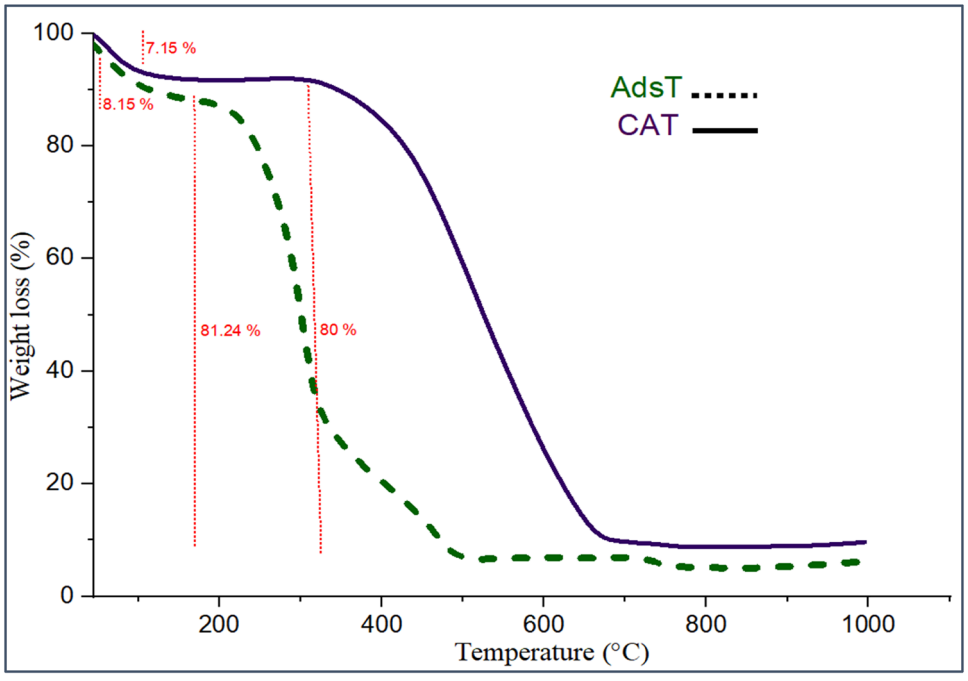

Figure 6: Thermograms (ATG) of AdsT and CAT.

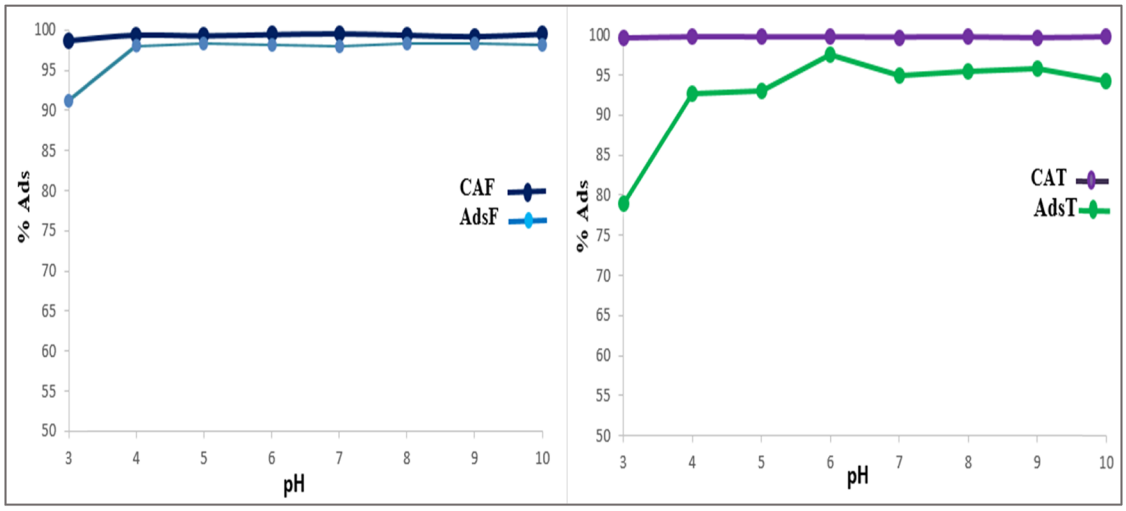

Figure 7: Effect of pH on adsorption of BG on CAF, AdsF, CAT, and AdsT (C_0 = 80 ppm, t = 30 min, m = 100 mg, V = 25 ml, and T = 25°C).

spectrophotometry was used to determine the dye concentration of the filtrate after filtration. Figure 7 shows that the adsorption rate of BG on AdsF was 91.25% at pH = 3, increasing to 98% at pH = 4, and remaining constant thereafter, while CAF reached a maximum and constant adsorption rate of 99% from pH = 3. For AdsT, the adsorption rate was 78.95% at pH = 3. It then increased with pH to reach 94.94%. For CAT, the adsorption percentage of BG was constant at 99% throughout the pH range studied. These results confirm that H^+ ions in an acidic environment reduce the contact between BG ions (cationic dye) and adsorbent sites. Conversely, at higher pH values, the H^+ concentration decreased, resulting in good interaction between dye ions and adsorbent surface sites. These results are almost identical to those obtained with cedar and mahogany sawdust-based adsorbents [19].

3.2.2 Contact time effect

Under stirring, 100 mg of sample was mixed with 25 ml of BG solution (80 ppm) for between 5 and 180 min. After filtration, the adsorption rate of BG increased within the first 15 min to 98.21% and remained stable for the next 165 min for AdsF, while for CAF the adsorption rate reached 97.5% within the first 5 min and remained almost constant. However, AdsT and CAT adsorption rates reached 95.47%

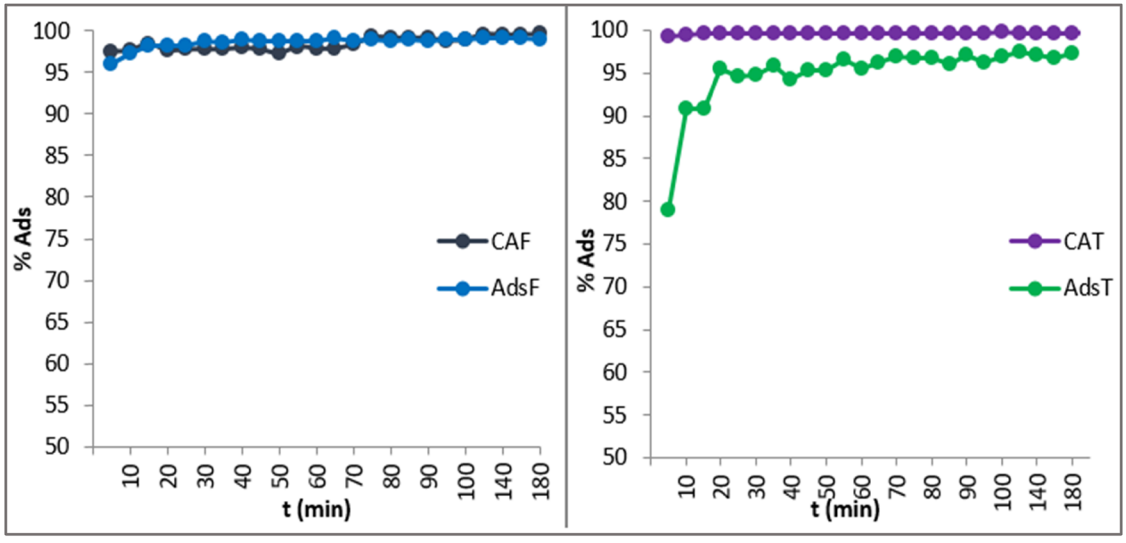

Figure 8: Contact time effect of BG adsorption on CAF, AdsF, CAT, and AdsT (C_0 = 80 ppm, m = 100 mg, V = 25 ml, and T = 25°C).

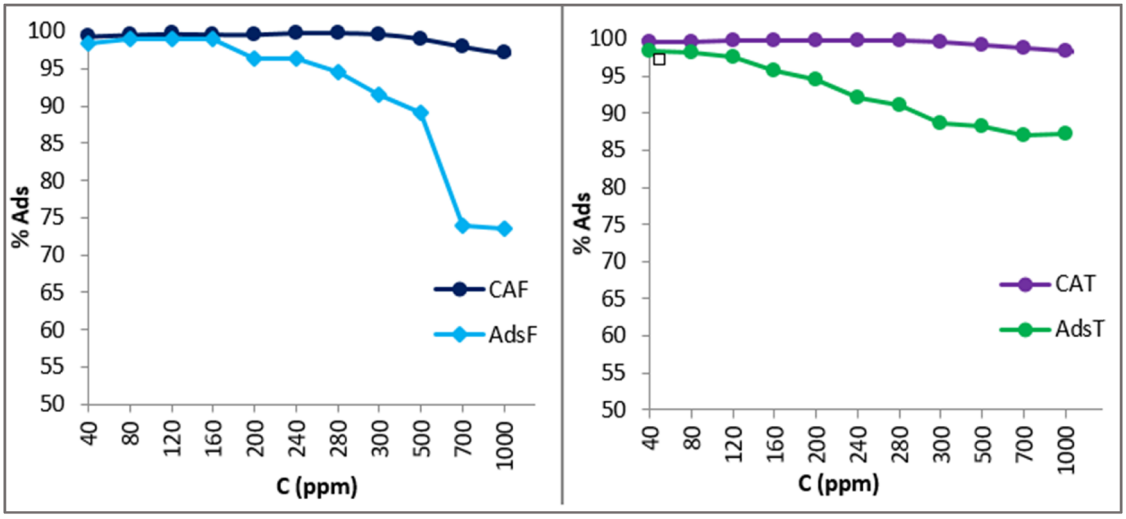

Figure 9: Initial concentration effect of BG adsorption on CAF, AdsF, CAT, and AdsT (t = 30 min, m = 100 mg, V = 25 ml, and T = 25°C).

during 20 min of contact and 99.30% during 5 min of contact, respectively (Figure 8).

3.2.3 Initial concentration effect

For 30 min, 100 mg of adsorbent was dispersed in 25 ml of BG solution, with initial BG concentrations varying from 40 to 1,000 ppm. The adsorption rate of the dye on the four adsorbents decreased with increasing concentration, as shown in Figure 9, due to saturation of active sites, thus with different kinetics. The AdsF adsorbent reached the first equilibrium at an initial concentration between 40 and 160 ppm with an average adsorption rate of 98.70%, the second equilibrium reached 92.72% in the 200–500 ppm range, and then the adsorption rate dropped to 74% with an initial concentration of 1,000 ppm. While CAF reached equilibrium at an initial concentration between 40 and 500 ppm with an average adsorption rate of 99.30%, it dropped to 97.26% for C_0 = 1,000 ppm. The AdsT curve shows an average adsorption rate of 98.30% at an initial concentration between 40 and 80 ppm, which then drops from 97.53 to 87% in the 120–1,000 ppm range. CAT reaches equilibrium at an initial concentration of between 40 and 500 ppm with an average adsorption rate of 99.32%, then increases to 97.9% at a concentration of 1,000 ppm. These results show that BG adsorption varies according to the colorant's initial concentration.

3.2.4 Adsorbent mass effect

A sample mass of 20–120 mg was distributed in 25 mL of BG solution with an 80 ppm concentration. The findings in Figure 10 demonstrate that the mass of the adsorbent

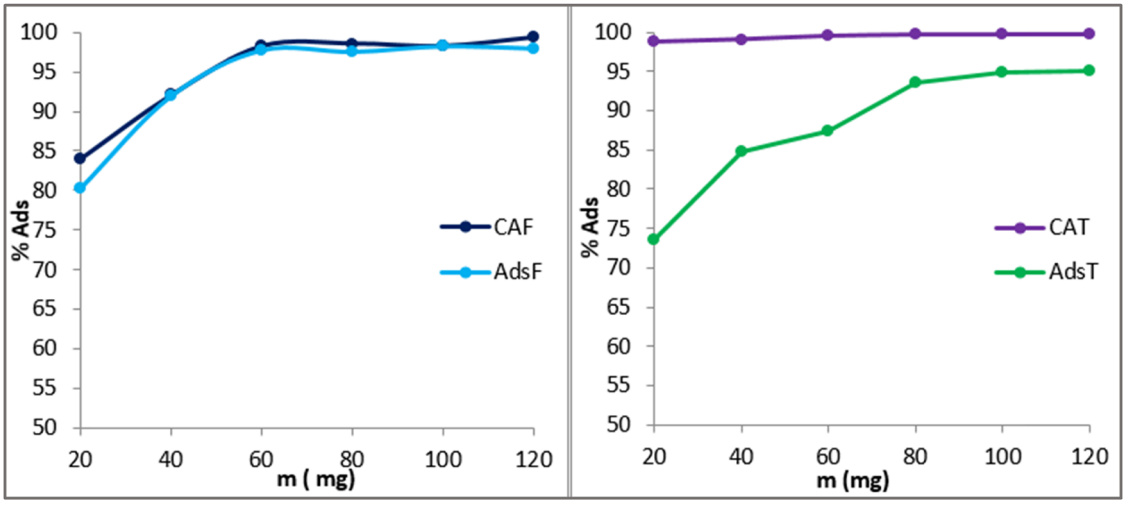

Figure 10: Adsorbent mass effect of BG adsorption on CAF, AdsF, CAT, and AdsT (t = 30 min, C_0 = 80 ppm, V = 25 ml, and T = 25°C).

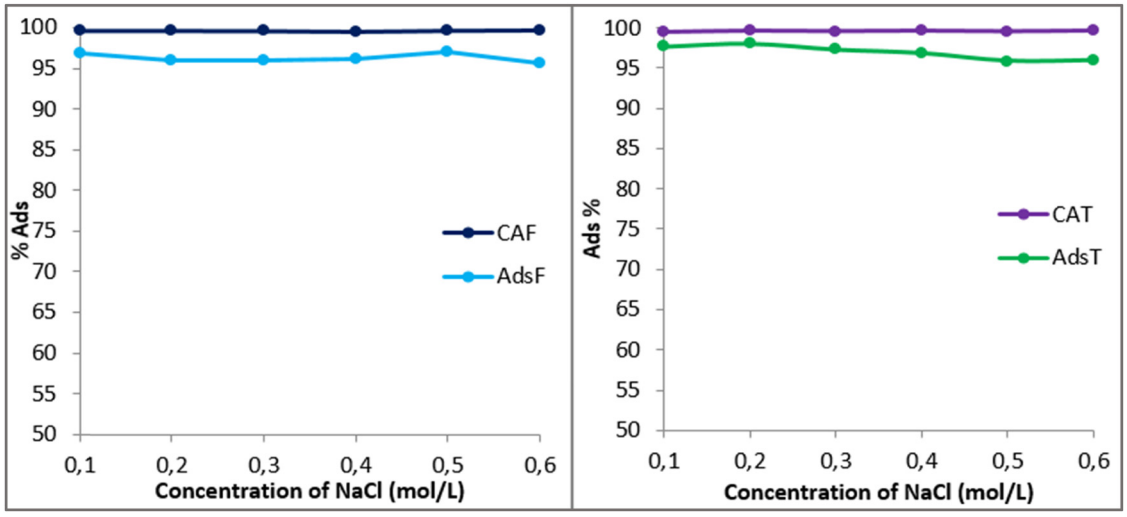

Figure 11: Effect of medium salinity on the adsorption rate of BG on CAF, AdsF, CAT, and AdsT (m = 100 mg, t = 30 min, C_0 = 80 ppm, V = 25 ml, and T = 25°C).

and the adsorption rate are proportionate. The BG adsorption rate increases from 80% to 98% when the mass of CAF and AdsF used increases from 20 to 60 mg, but beyond this range the adsorption rate remains constant. The adsorption rate for CAT reaches its maximum value of 99% at 20 mg and for AdsT it reaches 95% at 100 mg, then stabilizes. This increase in the adsorption rate of BG can be explained by the increase in the specific surface area involved.

3.2.5 Ionic strength effect

For 30 min, 100 mg of sample was stirred in 25 ml of 80 ppm BG solution at NaCl concentrations ranging from 0.1 to 0.6 M in 0.1 M steps. The obtained results indicate that the adsorption rate of BG remains constant with increasing NaCl concentration. As there is no competition for surface adsorption of Cl^- anions and BG cations in Figure 11, it can be concluded that ionic strength has no influence on the adsorption capacity. These results are consistent with the findings of previous research [6].

3.2.6 Temperature effect

Stirring for 30 min was used to disperse 100 mg of sample in 25 ml of a BG solution at a concentration of 80 ppm at temperatures ranging from 25 to 70°C. The results show

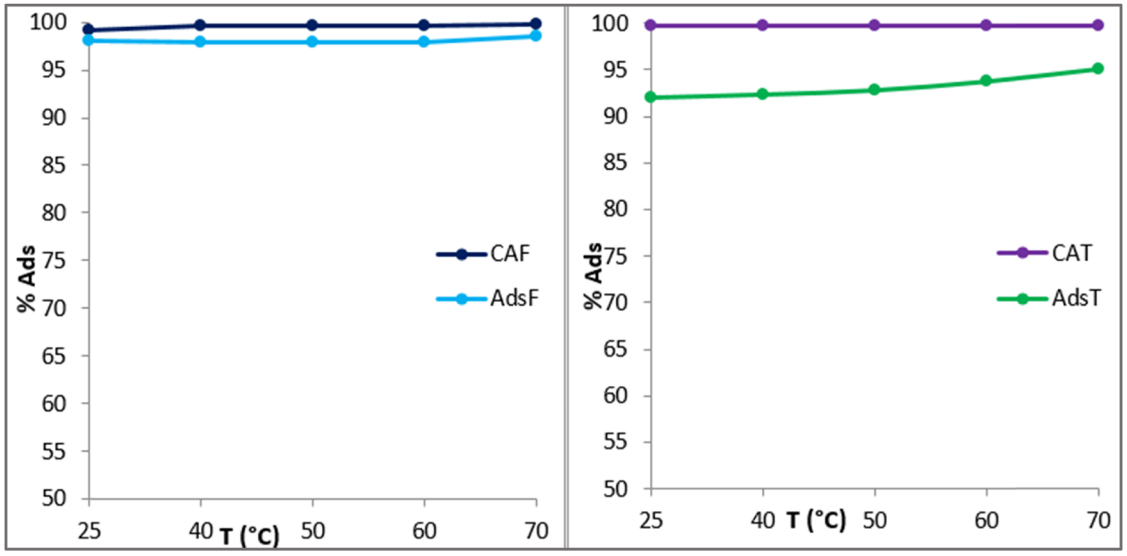

Figure 12: Effect of temperature on adsorption of BG on CAF, AdsF, CAT, and AdsT (m = 100 mg, t = 30 min, C_0 = 80 ppm, and V = 25 ml).

Table 5: Parameters of PFO and PSO BG adsorption kinetics on CAF, AdsF, CAT, and AdsT

Adsorbents	PFO			PSO			q_e exp (mg/g)
	K_1 (min^{-1})	R^2	q_e (mg/g)	K_2 ($g \cdot min^{-1} \cdot mg^{-1}$)	R^2	q_e cal (mg/g)	
CAF	0.0157	0.3247	0.50	0.0736	0.9999	19.96	19.92
AdsF	0.0196	0.5878	0.28	0.2466	1.0000	19.84	19.84
CAT	0.0096	0.4331	0.03	1.7928	1.0000	19.96	19.95
AdsT	0.0177	0.5600	0.98	0.0538	0.9999	19.53	19.49

that temperature has no significant effect on the adsorption rate (Figure 12).

3.3 Adsorption kinetics modeling

The obtained results for the kinetic modeling of the BG adsorption are shown in Table 5, where they show that the values of the R^2 correlation coefficient for the first-order model are far from 1, while they are quite close to unity for the second-order model. The quantities of dye adsorbed at equilibrium per gram of CAF, AdsF, CAT, and AdsT were calculated using the second-order model (q_e cal); however, they are extremely similar to the experimental values (q_e exp). This suggests that the second-order model describes the BG's adsorption kinetics. These outcomes resemble those of El Hajam et al., who demonstrated that the PSO model describes the BG adsorption process on cedar and mahogany sawdust [19].

3.4 Adsorption isotherm modeling

The results from the Langmuir and Freundlich models are used to calculate the maximum adsorption capacity and the adsorption parameters (Table 6). The regression coefficients show that the Langmuir isotherm best characterizes the BG adsorption mechanism on the four adsorbents, with linear regression coefficients R^2 on the order of 1. The results for cedar and mahogany sawdusts are comparable [19].

Table 6: BG adsorption parameters for CAF, AdsF, CAT, and AdsT using the Langmuir and Freundlich models

Models	Adsorbents	CAF	AdsF	CAT	AdsT
Langmuir	R^2	0.9681	0.9503	0.9663	0.9638
	q_{max}	250.00	172.41	270.27	161.29
	K_L	0.3125	0.0544	0.3394	0.0752
Freundlich	R^2	0.7824	0.9041	0.8355	0.8513
	K_f	53.40	22.04	58.53	16.04
	n_f	2.09	2.62	1.89	1.84

3.5 Comparative study of different quantities of dyes adsorbed from BG dyes with different eco-friendly and non-eco-friendly adsorbents

In the present study, the amount of dye adsorbed by each adsorbent and the most effective adsorbent for dye removal were determined by examining the adsorption of the BG dye on different types of prepared, neat, or activated adsorbents under constant operating conditions (C_0 = 80 ppm, m = 100 mg, V = 25 ml, T = 25°C, and t = 120–180 min). As presented in Table 7, CAT showed the highest amount of adsorbed dye for BG dye removal, followed by CAF, AdsF, and AdsT. Different quantities of the adsorbed dye q_e obtained for BG dye uptake by different adsorbents are greater than those obtained by different adsorbents presented in Table 7 from previous studies. These results allow us to conclude that the adsorbents used in this study, whether raw or activated, perform better than the other eco-friendly or non-eco-friendly adsorbents presented in Table 7. For this reason, cardoon waste remains a perfect precursor for the preparation of ecological adsorbents which are more effective for the treatment of water contaminated by synthetic organic dyes. Cardoon is also used in other fields, for example, in the extraction of phenolic compounds [2].

4 Conclusions

The properties of AdsF, AdsT, CAF, and CAT have been determined. Adsorption was examined in relation to the following variables: pH value (3–10), contact time (5–180 min), initial dye concentration (40–1,000 ppm), and adsorbent mass

Table 7: Comparison of different quantities of dye adsorbed reported by other researchers for BG dye removal with different eco-friendly and non-eco-friendly adsorbents

Adsorbent			Quantity of dye adsorbed q_e (mg/g)	Operating conditions	Reference
Non-eco-friendly adsorbents	$Cu_{0.5}Mn_{0.5}Fe_2O_4$ nanospinels		0.8900	pH = 2, C_0 = 100 ppm, t = 120 min, T = 50°C	[29]
	Pristine MOF-5		6.2500	m = 1.4 g, C_0 = 20 ppm, t = 2 h, T = 30 °C.	[30]
	Cellulose derivatives – $CuFe_2O_4$–zeolite	ZSM-5/CuF/CE	9.668	T = 20°C, t = 140 min, V = 25 ml, m = 10 mg, C_0 = 5 ppm	[31]
		ZSM-5/CuF/CEA	6.547		
Eco-friendly adsorbents	CAF		19.9200	C_0 = 80 ppm, m = 100 mg, V = 25 ml, T = 25°C, t = 180 min	Present study
	AdsF		19.8400	C_0 = 80 ppm, m = 100 mg, V = 25 ml, T = 25°C, t = 140 min	
	CAT		19.9500	C_0 = 80 ppm, m = 100 mg, V = 25 ml, T = 25°C, t = 180 min	
	AdsT		19.4900	C_0 = 80 ppm, m = 100 mg, V = 25 ml, T = 25°C, t = 120 min	
	Salix alba leaves		15.8900	pH = 6, m = 0.15 g, C_0 = 50 ppm, t = 3.5 h, T = 298 K	[32]
	Rambutan peels		9.6400	t = 24 h	[33]
	Tannin gel		8.5500	pH = 7	[34]
	Cedar		2.1523	C_0 = 50 ppm, agitation speed = 250 rpm, T = 25°C, pH = 6, m = 2 g,	[19,35]
	Mahogany		2.0189	t = 250 min, 100 µm < Φ < 500 µm	

C_0: initial concentration of BG, t: contact time, T: temperature, pH: pH of the solution, m: mass, V: volume, and Φ: particle mesh size.

(20–120 mg) of CAF, AdsF, CAT, or AdsT. The influence of the temperature of the reaction medium (20–70°C) and salinity on the adsorption process was studied. The maximum adsorption rate of BG was achieved between pH = 3 and pH = 10 for CAF and CAT. However, AdsF and AdsT reached their maximum adsorption rate between pH = 4 and pH = 10. The adsorption rate increased with the increase in the adsorbent mass; CAT reached its maximum value of 99% at 20 mg and AdsT 95% at 100 mg, for CAF and AdsF, the adsorption rate of BG increased from 80 to 98% when their masses increased from 20 to 60 mg. The adsorption rate of BG increased within the first 15 min to 98.21% and remained stable for the next 165 min for AdsF, while for CAF the adsorption rate reached 97.5% within the first 5 min and remained almost constant. However, AdsT and CAT adsorption rates reached 95.47% during 20 min of contact and 99.30% during 5 min of contact, respectively. The optimum initial concentration of BG was 80 ppm. The ionic strength and temperature had no major influence on dye adsorption. For all four adsorbents, the Langmuir model was well suited, based on the results of adsorption modeling using Freundlich and Langmuir isotherms. The PSO model best describes the adsorption kinetics of BG on CAF, AdsF, CAT, or AdsT, according to the evaluation of the adsorption kinetics using the PFO and PSO models. These results allow us to conclude that cardoon leaves or stems are excellent adsorbents for the adsorption of synthetic dyes.

Acknowledgements: This project was supported by Princess Nourah bint Abdulrahman University Researchers Supporting Project number (PNURSP2024R221), Princess Nourah bint Abdulrahman University, Riyadh, Saudi Arabia.

Funding information: This project was supported by Princess Nourah bint Abdulrahman University Researchers Supporting Project number (PNURSP2024R221), Princess Nourah bint Abdulrahman University, Riyadh, Saudi Arabia.

Author contributions: M.H.N.: methodology and writing – original draft; H.B. and M.E.H.: methodology; M.M.A. and M.E.H.: software and editing; F.B. and M.M.A.: funding acquisition and conceptualization; M.M.A., H.B., and F.B.: supervision and formal analysis. All authors have read and agreed to the published version of the manuscript.

Conflict of interest: The authors declare no conflicts of interest.

Data availability statement: All the data in the article are available from the corresponding author upon reasonable request. Samples of the compounds are not available from the authors at this time.

References

[1] Brás T, Paulino AFC, Neves LA, Crespo JG, Duarte MF. Ultrasound assisted extraction of cynaropicrin from Cynara cardunculus leaves: Optimization using the response surface methodology and the effect of pulse mode. Ind Crop Prod. 2020;150:112395.

[2] Garcia-Castello EM, Moratalla M, Reig M, Iborra-Clar MI, Iborra-Clar A, Rodriguez-Lopez AD. Clarification of the cardoon (Cynara cardunculus) blanching wastewater by ultrafiltration – study of membrane fouling and flux recovery after chemical cleaning. Separations. 2023;10:418.

[3] Alina-Ioana Gostina VYW. Edible flowers as functional food: A review on artichoke (Cynara cardunculus L.). Trends Food Sci Technol. 2018;86:381–91.

[4] Hajji Nabih M, Boulika H, El Hajam M, Alghonaim MI, Idrissi Kandri N, Alsalamah SA, et al. Successive solvent extraction, characterization and antioxidant activities of cardoon waste (leaves and stems) extracts: comparative study. Molecules. 2023;28:1129.

[5] Hajji Nabih M, Boulika H, El hajam M, Idrissi Kandri N, Zerouale A. Synthesis of an activated carbon based on cardoon waste and its comparison to a commercial carbon in terms of physicochemical characterization and organic dye adsorption performance. Key Eng Mater. 2023;954:41–54.

[6] Hajji Nabih M, El Hajam M, Boulika H, Chiki Z, Ben Tahar S, Idrissi Kandri N, et al. Preparation and characterization of activated carbons from cardoon "Cynara Cardunculus" waste: Application to the adsorption of synthetic organic dyes. Mater Today Proc. 2023;72:3369–79.

[7] El Hajam M, Idrissi Kandri N, Harrach A, Zerouale A. Adsorption of methylene blue on industrial softwood waste "cedar" and hardwood waste "mahogany": comparative study. Mater Today Proc. 2019;13:812–21.

[8] Boulika H, El Hajam M, Hajji Nabih M, Riffi Karim I, Idrissi Kandri N, Zerouale A. Definitive screening design applied to cationic & anionic adsorption dyes on Almond shells activated carbon: Isotherm, kinetic and thermodynamic studies. Mater Today Proc. 2023;72:3336–46.

[9] El Hajam M, Idrissi Kandri N, Plavan GI, Harrath AH, Mansour L, Boufahja F, et al. Pb^{2+} ions adsorption onto raw and chemically activated Dibetou sawdust: Application of experimental designs. J King Saud Univ-Sci. 2020;32:2176–89.

[10] El Hajam M, Idrissi Kandri N, Özdemir S, Plavan G, Ben Hamadi N, Boufahja F, et al. Statistical design and optimization of Cr (VI) adsorption onto Native and HNO_3/NaOH activated cedar sawdust using AAS and a response surface methodology (RSM). Molecules. 2023;28:7271.

[11] Monette F, Brière FG, Létourneau M, Duchesne M, Hausler R. Traitement des eaux usées par coagulation-floculation avec recirculation des boues chimiques: Performance générale et stabilité du procédé. Can J Civ Eng. 2000;27:702–18.

[12] Boulika H, Hajji Nabih M, El Hajam M, Idrissi Kandri N. Preparation of a photocatalytic activated carbon based on almond shell and Ag-ZnO: characterization and application to organic effluent treatment. Key Eng Mater. 2023;954:17–29.

[13] Boulika H, El Hajam M, Hajji Nabih M, Idrissi Kandri N, Zerouale A. Physico-chemical properties and valorization perspectives of almond residues (shells & hulls) in the northern Morocco: a comparative study. Biomass Convers Biorefinery. 2024;1–10.

[14] Hajji Nabih M, El Hajam M, Boulika H, Hassan MM, Idrissi Kandri N, Hedfi A, et al. Physicochemical characterization of cardoon 'cynara cardunculus' wastes (Leaves and stems): A comparative study. Sustain. 2021;13:1–12.

[15] Alongamo BAA, Ajifack LD, Ghogomu JN, Nsami NJ, Ketcha JM. Activated carbon from the peelings of cassava tubers (Manihot esculenta) for the removal of nickel(II) ions from aqueous solution. J Chem. 2021;2021:1–14.

[16] ElShafei GMS, ElSherbiny IMA, Darwish AS, Philip CA. Artichoke as a non-conventional precursor for activated carbon: Role of the activation process. J Taibah Univ Sci. 2017;11:677–88.

[17] Mamane OS, Zanguina A, Daou I, Natatou I. Préparation et caractérisation de charbons actifs à base de coques de noyaux de Balanites Eagyptiaca et de Zizyphus Mauritiana. la Société Ouest-Africaine Chim. 2016;41:59–67.

[18] Pinta M. Méthodes de référence pour la détermination des éléments minéraux dans les végétaux: Détermination des éléments Ca, Mg, Fe, Mn, Zn et Cu par absorption atomique. Oléagineux. 1973;28:87–92.

[19] El Hajam M, Idrissi Kandri N, Harrach A, et al. Adsorptive removal of brilliant green dye from aqueous solutions using cedar and mahogany sawdusts. Sci Study Res Chem Chem Eng Biotechnol Food Ind. 2019;20:395–409.

[20] Ho YS, McKay G. Sorption of basic dye from aqueous solution by pomelo. Chem Eng J. 1998;70:115–24.

[21] Rangabhashiyam S, Anu N, Selvaraju N. Sequestration of dye from textile industry wastewater using agricultural waste products as adsorbents. J Env Chem Eng. 2013;1:629–41.

[22] Matandabuzo M, Ajibade PA. Removal of metal ions from aqueous solutions using activated carbon prepared from zea mays stem. Sci Study Res Chem Chem Eng Biotechnol Food Ind. 2018;19:117–32.

[23] Lafi R, Montasser I, Hafiane A. Adsorption of congo red dye from aqueous solutions by prepared activated carbon with oxygen-containing functional groups and its regeneration. Adsorpt Sci Technol. 2019;37:160–81.

[24] Benadjemia M, Millière L, Reinert L, Benderdouche N, Duclaux L. Preparation, characterization and Methylene Blue adsorption of phosphoric acid activated carbons from globe artichoke leaves. Fuel Process Technol. 2011;92:1203–12.

[25] Boulika H, El Hajam M, Hajji Nabih M, Idrissi Kandri N, Zerouale A. Activated carbon from almond shells using an eco-compatible method: screening, optimization, characterization, and adsorption performance testing. RSC Adv. 2022;12:34393–403.

[26] Mokhtaryan S, Khodabakhshi A, Sadeghi R, Nourmoradi H, Shakeri K, Hemati S, et al. New activated carbon derived from Gundelia tournefortii seeds for effective removal of acetaminophen from aqueous solutions: Adsorption performance. Arab J Chem. 2023;16:105253.

[27] Namasivayam C, Kavitha D. IR, XRD and SEM studies on the mechanism of adsorption of dyes and phenols by coir pith carbon from aqueous phase. Microchem J. 2006;82:43–8.

[28] Ji W, Wang D, Guo J, Fei B, Gu X, Li H, et al. The preparation of starch derivatives reacted with urea- phosphoric acid and effects on fire performance of expandable polystyrene foams. Carbohydr Polym. 2019;233:115841.

[29] Hashemian S, Dehghanpor A, Moghahed M. Cu0. 5Mn0. 5Fe2O4 nano spinels as potential sorbent for adsorption of brilliant green. J Ind Eng Chem. 2015;24:308–14.

[30] Dahlan I, Obi CC, Razaman NS, Hasan HYA. Adsorptive decolorization of brilliant green dye in aqueous media using various modified MOF-5 adsorbents. Groundw Sustain Dev. 2024;101228.
[31] Katowah DF, Alzahrani HK. A new ternary nanocomposites-based cellulose derivatives-$CuFe_2O_4$-zeolite with ultra-high adsorption capacity for Brilliant Green dye treatment and removal from the aquatic environment. J Saudi Chem Soc. 2023;27:101764.
[32] Fiaz R, Hafeez M, Mahmood R. Removal of brilliant green (BG) from aqueous solution by using low cost biomass Salix alba leaves (SAL): thermodynamic and kinetic studies. J Water Reuse Desalin. 2020;10:70–81.
[33] Nor NM, Hadibarata T, Yusop Z, Lazim ZM. Removal of brilliant green and procionred dyes from aqueous solutionby adsorption using selected agricultural wastes. J Teknologi. 2015;74:117–22.
[34] Akter N, Hossain MA, Hassan MJ, Amin MK, Elias M, Rahman MM, et al. Amine modified tannin gel for adsorptive removal of Brilliant Green dye. J Environ Chem Eng. 2016;4:1231–41.
[35] El Hajam M, Idrissi Kandri N, Zerouale A. Batch adsorption of brilliant green dye on raw beech sawdust: equilibrium isotherms and kinetic studies. Moroccan J Chem. 2019;7:431–5.